Chemical Engineering Journal 499 (2024) 156225

Contents lists available at ScienceDirect

Chemical Engineering Journal

journal homepage: www.elsevier.com/locate/cej

Microwave-assisted chemical looping gasification of plastics for H_2-rich gas production

Wenming Fu, Yaning Zhang *, Weitao Cao, Wenke Zhao, Bingxi Li

School of Energy Science and Engineering, Harbin Institute of Technology (HIT), Harbin 150001, China

ARTICLE INFO

Keywords:
Microwave-assisted gasification
Chemical looping gasification
Plastic
Gas production
$NiFe_{20}O_x$ oxygen carrier

ABSTRACT

Microwave-assisted heating coupled with chemical looping gasification was first proposed for the recycling of plastics into H_2 rich gas, achieving a hydrogen conversion efficiency of up to 84.3%. In the experiment, plastic was initially decomposed into hydrocarbon volatiles, followed by the gasification reactions in the presence of an oxygen carrier under vacuum conditions for 10 min. Subsequently, air was introduced for wax removal and oxygen carrier recovery for another 10 min. This study evaluated the chemical looping gasification performances of polypropylene using oxygen carriers $Ni_aFe_bO_x$ with different Ni/Fe molar ratios (0, 1:40, 1:20, 1:10, 3:20, and 1:5). $NiFe_{20}O_x$ showed the highest gas yield of 81.3 mmol/g_{PP} with an H_2 yield of 46.0 mmol/g_{PP}. Among different microwave powers (590 W, 690 W, 790 W, 890 W, and 990 W), 890 W was identified as the ideal microwave power for maximum gas yield and H_2 yield. Microwave-assisted heating exhibited high efficiency, achieving a heating rate of 450 °C/min at 890 W, with the microwave oven consuming only 0.182 kWh of electrical power during the entire experiment. In the chemical looping gasification of various plastics (polypropylene, high-density polyethylene, low-density polyethylene, polystyrene, and plastics mixture) over $NiFe_{20}O_x$ under 890 W microwave power, polypropylene yielded the highest gas and H_2 production. This study provides a novel approach for efficiently recycling plastics, alleviating environmental pollution and contributing to energy sustainability.

1. Introduction

Plastic products are ubiquitous in modern society due to their affordability, malleability, and convenience, which have made them exceedingly popular among consumers. As global demand continues to rise, plastic production reached a substantial 400.3 million tonnes annually in 2022 [1]. However, their non-biodegradability and prohibitive recycling costs lead to significant environmental pollution and pose threats to human health [2]. Plastics often end up in landfills or the natural environment, where they can persist for centuries, releasing harmful chemicals and microplastics into ecosystems [3]. The most widely used types of plastics include polypropylene (PP), low-density polyethylene (LDPE), high-density polyethylene (HDPE), and polystyrene (PS), collectively constituting approximately 18.9%, 14.1%, 12.2%, and 5.2% of global plastic production, respectively [1]. This study focuses on these four types of plastics.

Gasification emerges as a promising method for recycling plastic waste by producing combustible gas [4]. However, the generated gas typically has a low heating value due to the inclusion of gasification agents such as air and carbon dioxide [5]. To address this issue, the chemical looping gasification method is proposed, wherein a solid oxygen carrier replaces conventional gasification agents [6]. The oxygen carrier can be reduced to provide oxygen atoms for the reaction with the plastic vapor, generating gas ($C_xH_y + MO_z \rightarrow (2x\text{-}z)\ CO + (z\text{-}x)\ CO_2 + (y/2)\ H_2 + M$) [7]. Subsequently, the reduced oxygen carrier can be regenerated by reacting with air or steam [8]. Metal oxides are commonly employed as oxygen carriers due to their cost-effectiveness, high reactivity in redox reactions, and substantial oxygen storage capacity [9]. For instance, Yao et al. [7] reported a carbon conversion efficiency of 99.03% and a gas production of 177.89 mmol/g_{PP} with a lower heating value of 11.35 MJ/Nm^3 from the chemical looping gasification of PP.

Chemical looping gasification of solid wastes typically operates at temperatures above 800 °C in an electric heating furnace to achieve high carbon conversion efficiency [10]. However, maintaining such high temperatures consumes considerable energy as electric heating not only heats the feedstocks but also the surrounding air. Microwave-assisted heating offers higher thermal efficiency compared to electrical heating due to its different heating mechanism [11]. Microwave heating utilizes

* Corresponding author.
E-mail address: ynzhang@hit.edu.cn (Y. Zhang).

https://doi.org/10.1016/j.cej.2024.156225

Available online 27 September 2024

Nomenclature

Abbreviations

AS	Air introduction stage
EN	Sum of vacuum stage and air introduction stage
Fe_3O_4	Ferrosoferric Oxide
HDPE	High-density polyethylene
HHV	Higher heating value
LDPE	Low-density polyethylene
MP	Mixed plastics
PP	Polypropylene
PS	Polystyrene
SA	Collected oxygen carriers after air introduction stage
SiC	Silicon carbide
SV	Collected oxygen carriers after vacuum stage
VS	Vacuum stage

Variables

a	is gas component obtained in the vacuum stage
A_{N2}	is the volumetric concentration of nitrogen in the air, vol.%
b	is gas component obtained in the air introduction stage
C_a	is carbon content in gas component a
C_b	is carbon content in gas component b
C_p	is carbon content in per gram plastic
H_a	is hydrogen content in gas component a
H_b	is hydrogen content in gas component b
HHV_a	is the HHV of gas component a, MJ/Nm^3
HHV_g	is the HHV of gas, MJ/Nm^3
H_p	is hydrogen content in per gram plastic
m_0	is weight of condensers, thermocouple, and connecting tubes before experiment, g
m_1	is weight of condensers, thermocouple, and connecting tubes after vacuum stage, g
m_2	is weight of quartz reactor, SiC, oxygen carrier, and plastic before experiment, g
m_3	is weight of quartz reactor, SiC, oxygen carrier, and wax after vacuum stage, g
M_a	is relative molecular mass of gas component a
m_f	is weight of feed plastic, g
v_a	is the volumetric concentration of gas component a in the vacuum stage, vol.%
v_b	is the volumetric concentration of gas component b in the air introduction stage, vol.%
v_{N2}	is volumetric concentration of nitrogen in the air introduction stage, vol.%
Y_a	is specific molar yield of gas component a, mmol/$g_{plastic}$
Y_b	is specific molar yield of gas component b, mmol/$g_{plastic}$
Y_{gam}	is specific molar yield of gas obtained in the air introduction stage, mmol/$g_{plastic}$
Y_{gv}	is gas yield in the vacuum stage, wt.%
Y_{gvm}	is specific molar yield of gas obtained in the vacuum stage, mmol/$g_{plastic}$
Y_{ov}	is oil yield in the vacuum stage, wt.%
η_C	is carbon conversion efficiency, %
η_H	is hydrogen conversion efficiency

electromagnetic waves to generate heat through mechanisms such as dipole rotation, ionic conduction, and interfacial polarization [12]. Moreover, materials exhibit varying microwave absorption capabilities [13], related to factors like dielectric constant, loss tangent, polarity, conductivity, and moisture content [14]. This method directly and uniformly heats materials, minimizing energy losses and enhancing overall efficiency [15]. Furthermore, microwave heating has a higher heating rate, which makes the reactions more vigorous, leading to a faster release of volatiles [16], thereby benefiting gas production [17]. An et al. [18] explored microwave-assisted chemical looping gasification of water hyacinth for syngas production, achieving a cold gas efficiency of 78.66% at 1000 W microwave power. However, research on microwave-assisted heating in chemical looping gasification of plastics remains absent.

Oxygen carriers played a pivotal role in the chemical looping gasification process [7], and extensive research has focused on identifying suitable oxygen carriers [19]. Ideal oxygen carriers should be cost-effective, mechanically stable, and exhibit excellent performance characteristics, including high oxygen transport capacity, high selectivity [20], and superior redox properties [21]. Metal oxides, including Ni, Fe, Mn, Cu [22], W, V [20] and Co [23], have been investigated extensively for chemical looping gasification. Iron-based oxygen carriers, such as Fe_3O_4, offer several advantages, such as abundant lattice oxygen, multiple oxidation states, and low cost [24]. For example, Xu et al. [25] investigated the chemical looping gasification of rice husk using Fe_3O_4 as the oxygen carrier, achieving a syngas yield of 46.99 mmol/g biomass. Iron oxides also exhibit favorable microwave absorption properties [26], making them compatible with microwave-assisted heating in chemical looping gasification. Fan et al. [13] studied the microwave heating performance of Fe_3O_4, achieving an instantaneous heating rate of up to 289.2 °C/min at 650 W microwave power, with an average heating rate of approximately 125 °C/min up to 1000 °C. However, Fe-based oxygen carriers are susceptible to sintering, which can negatively impact the gasification process and gas production [22]. To mitigate these challenges, Fe-based oxygen carriers are often modified with other oxides [27]. Additionally, combining two active metals can synergistically enhance catalytic performance beyond that of individual metals [28]. For instance, Qiu et al. [29] demonstrated that $CoFeO_x$ as an oxygen carrier achieved a H_2 yield of 11.17 mmol/g in chemical looping H_2 production from water splitting, surpassing Fe_2O_3 (7.61 mmol/g). The synergistic effects of Co doping into Fe_2O_3, validated through temperature-programmed reduction analysis, were shown to promote the reduction of Fe. Huang et al. [30] examined the chemical looping gasification of biomass char using $NiFe_2O_4$, which exhibited superior char gasification performance with a carbon conversion efficiency of 88.12%, significantly higher than that of individual Fe_2O_3 or a mechanical mixture of Fe_2O_3 and NiO, due to the Fe/Ni synergistic effect. Despite these advancements, research on identifying oxygen carriers suitable for microwave-assisted heating in chemical looping gasification of plastics is lacking.

H_2 is a clean energy carrier with significant potential to mitigate environmental challenges, and it is the primary gas product of chemical looping gasification of plastics [7]. Key parameters that influence H_2 yield include reaction temperature, microwave power, oxygen carrier type, and plastic type. Reaction temperature plays a crucial role in the chemical looping gasification process, as higher temperatures promote the cracking of large molecules [8]. Previous studies have demonstrated that increasing temperature generally results in higher gas yields and greater H_2 production [31]. Similarly, higher microwave power leads to faster heating, which accelerates the decomposition of plastic waste and promotes the release of hydrogen and other volatiles [32]. However, an optimal balance must be maintained to avoid issues such as localized overheating or inefficient energy use. The selection of a suitable oxygen carrier is critical for facilitating the redox reactions in the gasification process [33]. Modifications to oxygen carriers, such as doping with Ni or Co, can further enhance H_2 production by improving catalytic performance [20]. Additionally, different types of plastics have varying hydrogen content and chemical structures with differing bond energies,

which influence the gasification process and H_2 yield [34]. To the best of the authors' knowledge, no study has investigated the influences of microwave power, oxygen carrier, and plastic type on the microwave-assisted chemical looping gasification of plastics. Therefore, it is of great interest to explore how these factors affect H_2-rich gas production in this process.

In this study, Ni was incorporated onto Fe_3O_4 through wet impregnation to produce $Ni_aFe_bO_x$ (where a and b represent the Ni/Fe molar ratio). The microwave-assisted heating coupled with chemical looping gasification of plastics was investigated using $Ni_aFe_bO_x$ as the oxygen carrier to produce high-quality gas. Various Ni/Fe molar ratios (0, 1:40, 1:20, 1:10, 3:20, and 1:5) and different microwave powers (590 W, 690 W, 790 W, 890 W, and 990 W) were examined to optimize the Ni/Fe molar ratio and microwave power, and to explore their effects on gas production. Using $NiFe_{20}O_x$ with a 1:20 Ni/Fe molar ratio (the optimal oxygen carrier) at a microwave power of 890 W (the optimal microwave power), the microwave-assisted chemical looping gasification of PP, PS, LDPE, HDPE, and mixed plastics (MP) was performed to evaluate their performance in gas production.

2. Materials and methods

2.1. Materials

The plastics used in this study, including pure PP, LDPE, HDPE, and PS particles, were sourced from China Shenhua Coal to Liquid and Chemical Co., Ltd. Silicon carbide (SiC) obtained from Qinghe Andi Metal Materials Co., Ltd., was used as microwave absorbent with a particle size range of 0.25–0.85 mm. Ferrosoferric Oxide (Fe_3O_4), acquired from Nangong Xindun Alloy Welding Material Spraying Co., Ltd., served as the support material for the oxygen carriers due to its widespread availability and excellent microwave absorption properties. Nickel nitrate hexahydrate ($Ni•(NO_3)_2·6H_2O$), provided by Sinopharm Chemical Reagent Co., Ltd., was utilized as the nickel source.

2.2. Synthesis method of oxygen carries

Oxygen carriers with different Ni/Fe molar ratios of $Ni_aFe_bO_x$ were synthesized using the wet impregnation method. The preparation procedure involved dissolving a predetermined quantity of $Ni•(NO_3)_2·6H_2O$ in 80 ml of deionized water, followed by the addition of 15.47 g Fe_3O_4. The mixture was agitated at 80 °C and 1000 rpm for 4 h in a magnetic stirring water bath to ensure homogenization. Subsequently, it was oven-dried at 105 °C for 24 h to evaporate all the water. The dried material was then crushed into a powder and calcined in a muffle furnace under an oxidative atmosphere at 550 °C for 5 h. Then the oxygen carriers were sieved using standard screens, with particle sizes ranging from 0.074 to 0.096 mm.

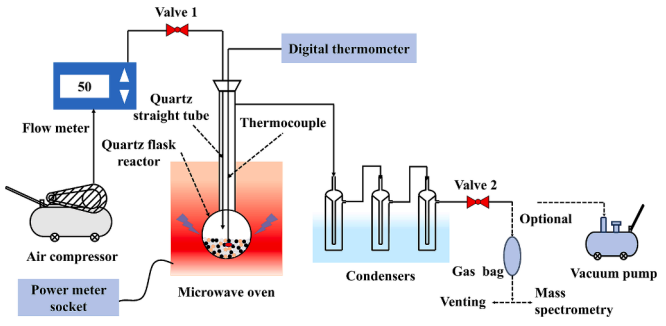

Fig. 1. Schematic diagram of the microwave-assisted chemical looping gasification system.

2.3. Experimental procedures

Fig. 1 illustrates the schematic diagram of the microwave-assisted chemical looping gasification system, which comprises a microwave oven, a power meter socket, a gas supply system, a temperature measuring system, a quartz flask reactor, a gas bag, condensers, connecting tubes, and valves. The cavity of the microwave oven (0 ~ 1000 W, 2450 MHz) measures 300 mm in length, 300 mm in width, and 350 mm in height. A 30 mm diameter hole is fabricated on the upper surface of the microwave oven for inserting a connecting tube. A 40 mm high pipe seal is placed above the hole to minimize microwave leakage. The power meter socket was used to measure the microwave oven's electrical energy consumption during the experiment. The gas supply system, which includes a flow meter, an air compressor, and a quartz straight tube, was used to supply air to the quartz flask reactor. The temperature measuring system, consisting of a K-type thermocouple and a digital thermometer, was employed to measure the temperature of the feedstocks. The quartz flask reactor, with a chamber volume of 100 ml, was used to contain the feedstocks. At the quartz flask reactor's outlet, three condensing tubes immersed in an ice-water mixture, were placed in series to cool the heavy volatiles and collect the condensable oil. A gas bag connected to the outlet of the condensers was used to collect the non-condensable gas. Two valves were used to control the reactor environment by opening and closing as needed.

Each experiment was repeated at least twice to ensure data reproducibility. Throughout the study, 1-g plastic, 6-g oxygen carrier, and 12-g SiC were fixed based on the pre-experiments. SiC possessed excellent microwave absorption ability and was used to absorb and convert more microwaves into heat to improve thermal efficiency. The experiment was divided into two stages: the vacuum stage and the air introduction stage. In the vacuum stage, the condensers, thermocouple, quartz straight tube, quartz flask reactor, and connecting tubes were initially weighed. The plastic particles, oxygen carriers, and SiC were weighed separately, then mixed uniformly and placed in the quartz flask reactor. The experimental system was connected as shown in Fig. 1, with insulation cotton filled in the microwave oven to reduce heat loss. Valve 1 was turned off and valve 2 was turned on. The experimental system was vacuumed with a vacuum pump for ten minutes. Then valve 2 was turned off and the vacuum pump was replaced with a gas bag. The microwave oven was started at the designed microwave power. When the temperature of the feedstock reached 900 °C, it was maintained within the range of 880–920 °C by turning the microwave oven on and off. After ten minutes, the microwave oven and valve 2 were turned off, and the gas bag was removed. Once the temperature of feedstock cooled below 100 °C, the condenser tubes, thermocouple, quartz straight tube, quartz flask reactor, and connecting tubes were weighed again. In the air introduction stage, the experimental system was reconnected as shown in Fig. 1. Valve 1 was turned off and valve 2 was turned on. The experimental system was vacuumed for ten minutes, then valve 2 was turned off and the vacuum pump was replaced with a new gas bag. The microwave oven was started again. Once the temperature reached 900 °C, the air compressor, valve 1, and the flow meter set at 50 ml/min were turned on. The temperature was maintained within the range of 880–920 °C by turning the microwave oven on and off. After ten minutes of air inlet, the microwave oven, valve 1, and valve 2 were turned off, and the gas bag was removed. When the temperature cooled below 100 °C, the condenser tubes, thermocouple, quartz straight tube, quartz flask reactor, and connecting tubes were weighed again. Finally, the spent oxygen carrier was collected for characterization, and the gas components in the two gas bags were analyzed using mass spectrometry.

2.4. Characterization methods

The produced oil weight was determined by assessing the weight variance of the condensers, thermocouple, and connecting tubes before and after the experiment. The produced gas weight was calculated by

subtracting the oil weight from the sum of the plastic particles' weight and the weight reduction of the oxygen carriers. These calculations are detailed in Equations (1), and (2).

$$Y_{ov} = \frac{m_1 - m_0}{m_f} \times 100\text{wt.\%} \quad (1)$$

$$Y_{gv} = \frac{m_2 - m_3}{m_f} \times 100\text{wt.\%} - Y_{ov} \quad (2)$$

where:

Y_{ov}	is oil yield in the vacuum stage, wt.%
Y_{gv}	is gas yield in the vacuum stage, wt.%
m_0	is weight of condensers, thermocouple, and connecting tubes before experiment, g
m_1	is weight of condensers, thermocouple, and connecting tubes after vacuum stage, g
m_2	is weight of quartz reactor, SiC, oxygen carrier, and plastic before experiment, g
m_3	is weight of quartz reactor, SiC, oxygen carrier, and wax after vacuum stage, g
m_f	is weight of feed plastic, g

The molar gas yield in the vacuum stage and the air introduction stage was calculated using Equation (3) and Equation (4), respectively.

$$Y_{gvm} = \frac{1000 Y_{gv}}{\sum_a v_a M_a} \quad (3)$$

$$Y_{gam} = \frac{500 A_{N_2}}{22.4 m_f v_{N_2}} \quad (4)$$

where:

a	is gas component obtained in the vacuum stage
M_a	is relative molecular mass of gas component a
Y_{gvm}	is specific molar yield of gas obtained in the vacuum stage, mmol/$g_{plastic}$
Y_{gam}	is specific molar yield of gas obtained in the air introduction stage, mmol/$g_{plastic}$
A_{N2}	is the volumetric concentration of nitrogen in the air, vol.%
v_a	is the volumetric concentration of gas component a in the vacuum stage, vol.%
v_{N2}	is volumetric concentration of nitrogen in the air introduction stage, vol.%

The molar gas yield of each gas component in the vacuum stage and air introduction stage was calculated using Equation (5), and Equation (6), respectively.

$$Y_a = Y_{gvm} \times v_a \quad (5)$$

$$Y_b = Y_{gam} \times v_b \quad (6)$$

where:

b	is gas component obtained in the air introduction stage
Y_a	is specific molar yield of gas component a, mmol/$g_{plastic}$
v_b	is the volumetric concentration of gas component b in the air introduction stage, vol.%
Y_b	is specific molar yield of gas component b, mmol/$g_{plastic}$

The higher heating value (HHV) of the gas was calculated using Equation (7). The carbon conversion efficiency and hydrogen conversion efficiency were calculated using Equations (8), and **(9)**, respectively.

$$HHV_g = \sum_a HHV_a v_a \quad (7)$$

$$\eta_C = \frac{\sum_a Y_a C_a + \sum_b Y_b C_b}{C_p} \times 100\% \quad (8)$$

$$\eta_H = \frac{\sum_a Y_a H_a + \sum_b Y_b H_b}{H_p} \times 100\% \quad (9)$$

where:

HHV_g	is the HHV of gas, MJ/Nm^3
HHV_a	is the HHV of gas component a, MJ/Nm^3
η_C	is carbon conversion efficiency, %
C_a	is carbon content in gas component a
C_b	is carbon content in gas component b
C_p	is carbon content in per gram plastic
η_H	is hydrogen conversion efficiency
H_a	is hydrogen content in gas component a
H_b	is hydrogen content in gas component b
H_p	is hydrogen content in per gram plastic

The surface morphology of the raw oxygen carriers was investigated using a Scanning Electron Microscope (SEM). The crystalline composition of the oxygen carriers—including the raw oxygen carriers, the spent oxygen carriers after the vacuum stage, and the spent oxygen carriers after the air introduction stage—was determined using X-Ray Powder Diffraction (Empyrean Intelligent X-ray Diffraction System) over the 2θ range of 0° to 90°, with a step size of 0.167°. It was used to confirm the loading of Ni on Fe_3O_4 and identify changes in the crystalline components following the vacuum and air introduction stages.

3. Results and discussion

3.1. Characterization of oxygen carriers

3.1.1. Surface morphology

The surface morphologies of the oxygen carriers are presented in Fig. 2. SEM images showed that Ni loading did not alter the structural framework of Fe_3O_4. Additionally, it was observed that Ni was primarily loaded on the surface of the oxygen carrier, and as the Ni ratio increased, more Ni was encapsulated on the surface of Fe_3O_4.

3.1.2. Crystal structure

Fig. 3 shows the XRD spectra of the oxygen carriers. For fresh Fe_3O_4, peaks corresponding to Fe_3O_4 (COD #9009768) were detected. For the collected Fe_3O_4 after the vacuum stage, peaks corresponding to Fe (#4113941), $Fe_{3.78}O_4$ (#1541150), and Fe_3O_4 (#9009770) were detected. The appearance of Fe and $Fe_{3.78}O_4$ was attributed to the reactions between Fe_3O_4 and the generated hydrocarbon vapors, where some lattice oxygens from Fe_3O_4 combined with the hydrocarbons, producing Fe and $Fe_{3.78}O_4$. For the collected Fe_3O_4 after the air introduction stage, peaks corresponding to Fe (#1100108), $Fe_{3.78}O_4$ (#1011168), Fe_2O_3 (#2108028), and Fe_3O_4 (#9009768) were detected. The appearance of Fe_2O_3 was attributed to the oxidation of Fe (#1100108) or $Fe_{3.78}O_4$ (#1011168) by O_2. For fresh $NiFe_{20}O_x$, peaks corresponding to $NiFe_2O_4$ (#5910064), NiO_2 (#9012319), Fe_2O_3 (#9015065), and Fe_3O_4 (#1532800) were detected. The presence of Fe_2O_3 was due to the oxidation of Fe_3O_4 by O_2 during the calcination process in the muffle furnace. For the collected $NiFe_{20}O_x$ after the vacuum stage, peaks corresponding to Fe (#9013472), Ni (#9013029), $Fe_{3.66}O_4$ (#1541151), FeO (#9008636), $Ni_{0.58}Fe_{1.42}$ (#1524199), and Fe_3O_4 (#9002026) were detected. The presence of Fe, $Fe_{3.66}O_4$, and FeO was attributed to the reduction of Fe_2O_3 or Fe_3O_4 by the generated hydrocarbon vapors, and Ni and $Ni_{0.58}Fe_{1.42}$ were derived from NiO_2 and $NiFe_2O_4$. For the collected $NiFe_{20}O_x$ after the air introduction stage, peaks corresponding to Fe (#4113941), Ni (#2100652), Fe_2O_3 (#9000139), FeO (#9008636), and Fe_3O_4 (#9002321) were detected. The presence of Fe_2O_3 was due to the oxidation of FeO or Fe by O_2.

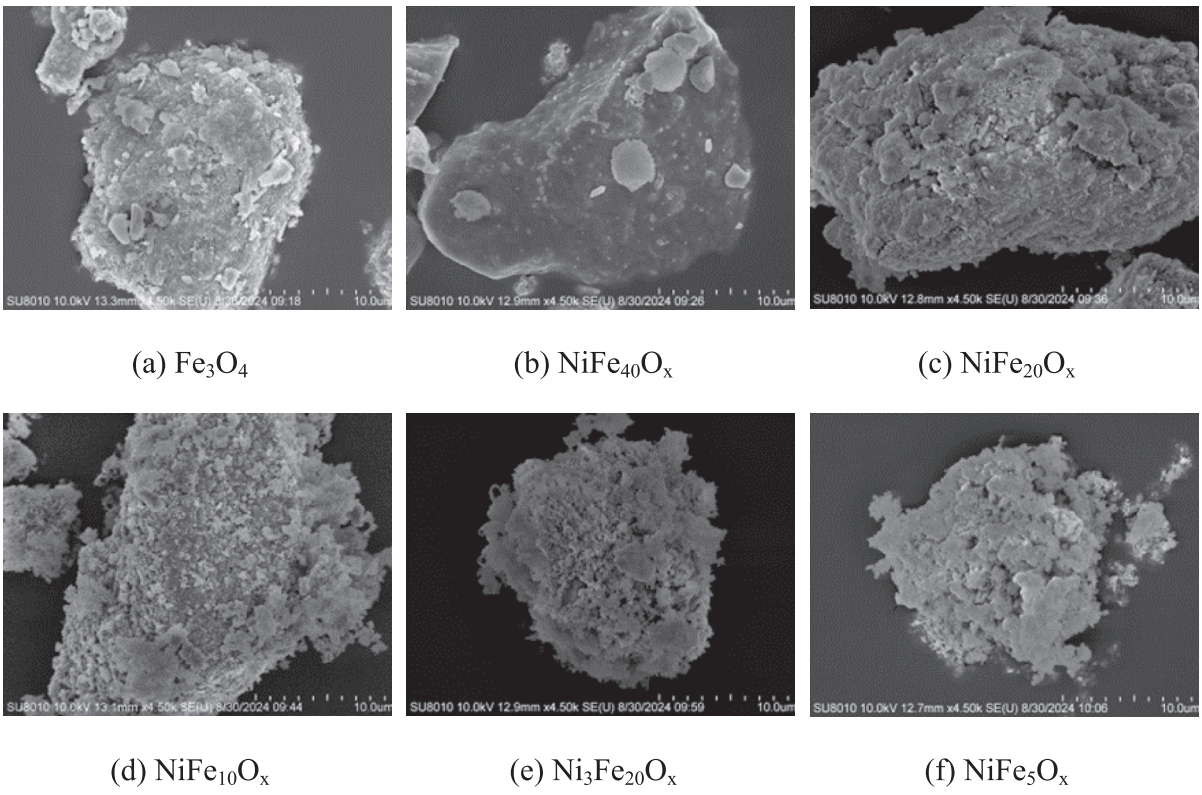

Fig. 2. SEM images of different oxygen carriers.

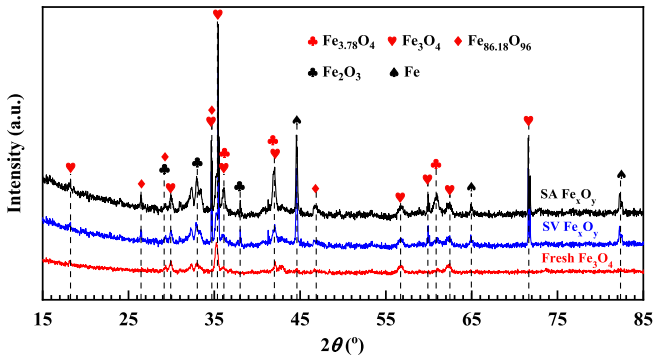

(a) Fe_3O_4

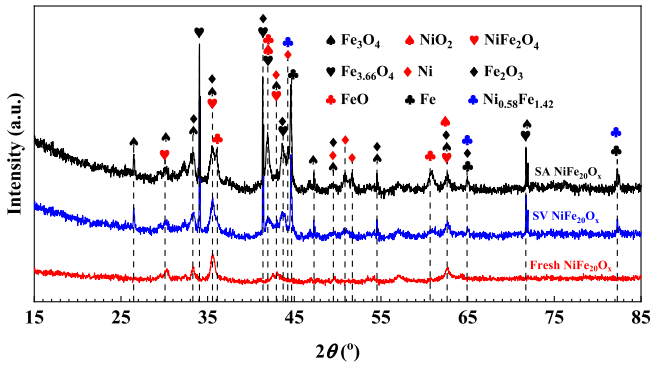

(b) $NiFe_{20}O_x$

Fig. 3. XRD spectra of fresh and spent oxygen carriers (SV: collected after vacuum stage, SA: collected after air introduction stage).

3.2. *Effect of nickel loading molar ratio*

The molar ratio of Ni loaded onto the oxygen carriers significantly influenced the experimental process. It notably affected the heating rate by altering the dielectric loss capacity and microwave absorption ability [35], and it also impacted the reactivity of the oxygen carriers by increasing the number of active sites, which promotes the cracking of plastic volatiles [36]. Therefore, it was essential to detail the effect of the Ni/Fe molar ratio on gas yield, gas components, and carbon conversion efficiency. A dedicated study was conducted on the chemical looping gasification of PP using $Ni_aFe_bO_x$ as the oxygen carrier with varying Ni/Fe molar ratios (0, 1:40, 1:20, 1:10, 3:20, and 1:5) to elucidate the effect of its influence on gas production. The experimental temperature was fixed at 900 °C, as higher temperatures favor gas production [31]. Microwave power was set at 890 W based on preliminary experiments. The results are presented in Fig. 4.

3.2.1. *Microwave heating performances*

Fig. 4 **(a)** shows the microwave heating performances of the feedstocks using $Ni_aFe_bO_x$ as oxygen carrier with different Ni/Fe molar ratios (0, 1:40, 1:20, 1:10, 3:20, and 1:5). To enhance thermal efficiency, SiC was added to each group to improve the heating rate. The temperature of the feedstocks increased from room temperature to 900 °C in 1.5–2.5 min, with heating rates ranging from 360 to 600 °C/min. Fe_3O_4 achieved the lowest heating rate, while $Ni_3Fe_{20}O_x$ achieved the highest. $Ni_aFe_bO_x$ demonstrated higher heating rate than Fe_3O_4, attributed to the mixture of the two metals promoting the generation of microwave plasma with increased heating efficiency [37]. In addition, transition metal oxides can generate defects and oxygen vacancies at high temperatures, which acted as dipole centers to induce dipole polarization relaxation [35]. The incorporation of varying quantities of Ni onto Fe_3O_4 changed its physical characteristics, thereby altering the dielectric loss capacity and affecting the microwave absorption ability. Due to the poor microwave absorption ability of PP, its temperature was initially lower compared to SiC

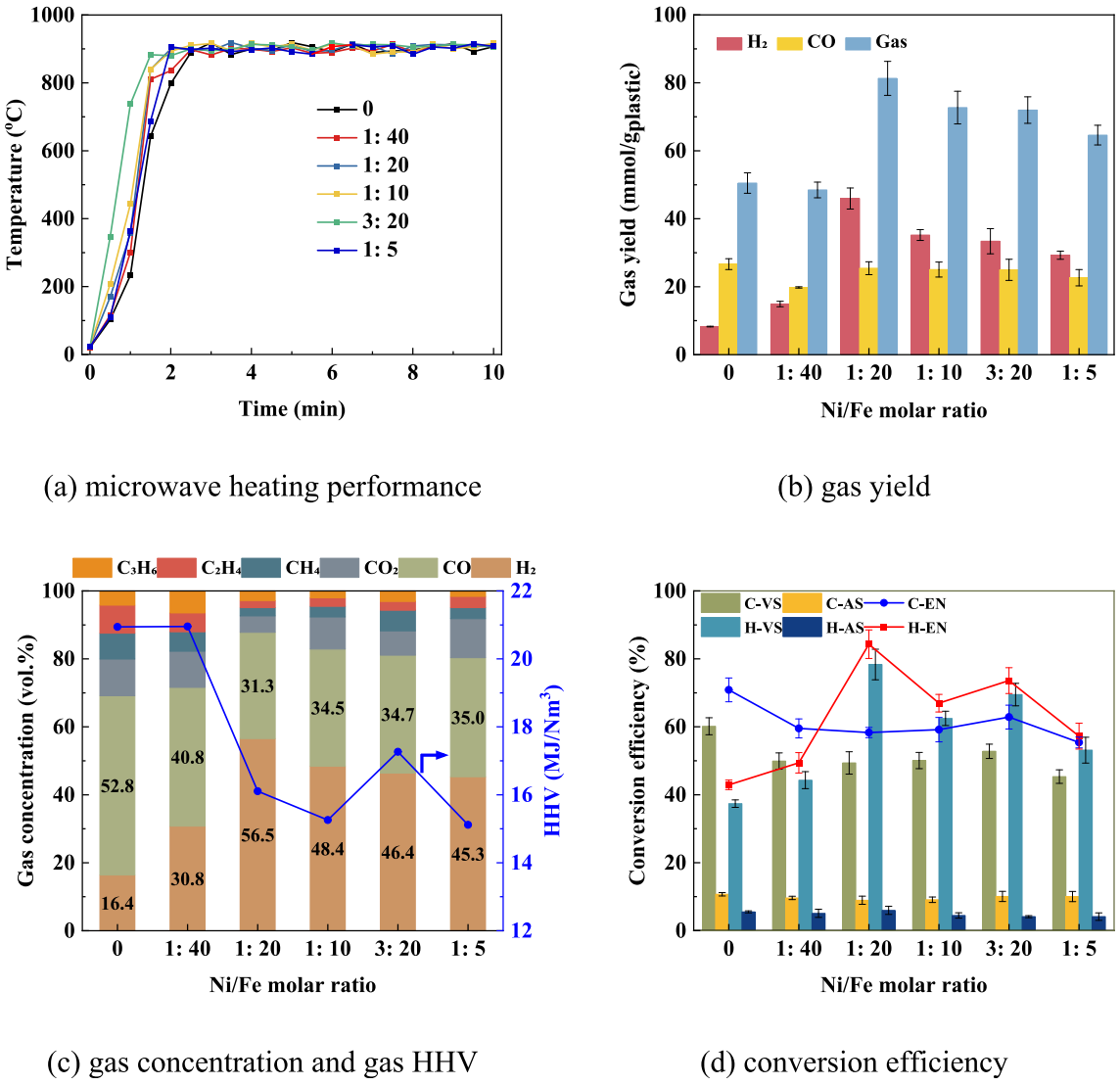

Fig. 4. Experimental results obtained from microwave-assisted chemical looping gasification of PP over $Ni_aFe_bO_x$ with different Ni/Fe molar ratios (VS: vacuum stage, AS: air introduction stage, EN: sum of vacuum stage and air introduction stage).

and the oxygen carrier, but it increased rapidly due to the heating from SiC and the oxygen carrier. This resulted in a temperature gradient from the oxygen carrier to the PP, aligning with the mass transfer direction, which was beneficial for plastic degradation, as demonstrated by a previous study [38].

3.2.2. *Products distribution*

Fig. 4 **(b)** shows the H_2 yield, CO yield, and gas yield obtained from the microwave-assisted chemical looping gasification of PP using $Ni_aFe_bO_x$ as the oxygen carrier with different Ni/Fe molar ratios. The oil yield is shown in Table 1. The gas yield and oil yield varied within the ranges of 48.5–81.3 mmol/g_{PP} and 23.3–41.9 wt.%, respectively. The H_2 yield and CO yield varied within the ranges of 8.3–46.0 mmol/g_{PP} and 17.4–26.6 mmol/g_{PP}, respectively. In the absence of Ni incorporation, a gas yield of 50.5 mmol/g_{PP} and an oil yield of 26.7 wt.% were obtained. At a Ni/Fe molar ratio of 1:40, the gas yield decreased to 48.5 mmol/g_{PP} while the oil yield increased to 41.9 wt.%. The incorporation of Ni increased the H_2 yield from 8.3 to 14.9 mmol/g_{PP}, as it increased the active sites and the activity of the oxygen carrier for H_2 production [39], which has been confirmed by many previous studies [40]. Although H_2 yield remained low, the increase in H_2 yield raised the unsaturation degree of the residues, thereby improving the oil yield and decreasing the CO yield. As the Ni/Fe ratio increased to 1:20, gas yield and H_2 yield increased significantly from 48.5 to 81.3 mmol/g_{PP} and from 14.9 to 46.0 mmol/g_{PP}, respectively. This was attributed to: (a) increased heating rate compared to $NiFe_{40}O_x$, promoting cleavage of C-H bonds and C-C bonds, and the yield of small molecules [32], and (b) more Ni providing additional active sites for C-H bond cleavage [36]. The lowest oil yield was due to the significant increase in H_2 yield, which promoted the generation of more free carbons [41], thereby reacting with the oxygen carrier and increasing the CO yield from 19.8 to 25.4 mmol/g_{PP}. With higher Ni molar ratios, both H_2 and gas yields decreased, likely due

Table 1
Oil yields of microwave-assisted chemical looping gasification of plastics at different experimental parameters.

Ni/Fe molar ratio	Oil yield (wt.%)	Microwave power (W)	Oil yield (wt.%)	Plastic type	Oil yield (wt.%)
0	26.7	590	40.7	LDPE	25.2
1: 40	41.9	690	36.5	HDPE	29.3
1: 20	23.3	790	32.0	PS	70.0
1: 10	31.5	890	23.3	PP	23.3
3: 20	32.1	990	42.9	MP	44.7
1: 5	33.7	/	/	/	/

to excess Ni obstructing the active sites on the oxygen carrier [42], as observed in the SEM images in Fig. 2, thereby inhibiting the catalytic activity of Fe_3O_4. As a result of the reduction in H_2 yield and free carbon, the CO yield decreased slightly. Due to the addition of the oxygen carrier, the gas yield (81.3 mmol/g_{PP}) and H_2 yield (46.0 mmol/g_{PP}) improved significantly compared with the microwave pyrolysis of PP at 900 °C, which produced 21.8 mmol/g_{PP} gas and 1.1 mmol/g_{PP} H_2 [43]. However, the obtained gas yield and H_2 yield were lower than those from chemical looping gasification of PP with steam introduced (gas yield 129.90 mmol/g_{PP}, H_2 yield 95.23 mmol/g_{PP}) [7], as steam significantly enhanced the gas production while reducing oil yield ($C_yH_z + yH_2O \rightarrow yCO + (y + z/2)\ H_2$, $C + H_2O \rightarrow CO + H_2$, $CO + H_2O \rightarrow CO_2 + H_2$, and $3Fe + 4H_2O \rightarrow Fe_3O_4 + 4H_2$) [44]. Despite the gas yield was lower in this study, the absence of steam simplified the experimental system and reduced energy consumption. Additionally, steam was typically introduced with the inert carrier gas to ensure uniform distribution [45], which diluted the produced gas, thereby reducing its quality and HHV values.

3.2.3. Gas compositions

Fig. 4 **(c)** shows the gas components and gas HHV obtained from the chemical looping gasification of PP using $Ni_aFe_bO_x$ as the oxygen carrier with different Ni/Fe molar ratios. The volume concentrations of H_2, CO, CO_2, CH_4, C_2H_4, and C_3H_6 varied within the ranges of 16.4–56.5%, 31.3–52.8%, 4.8–10.8%, 2.4–7.6%, 2.1–8.3%, and 1.6–6.5%, respectively. The main components of the gas were H_2 and CO, attributed to the addition of the oxygen carrier. With the incorporation of Ni, the H_2 concentration increased significantly, resulting from the enhancement of C-H bond breakage by Ni [36]. As the ratio of Ni increased, the H_2 concentration initially increased and then decreased, with the highest H_2 concentration obtained at a Ni/Fe molar ratio of 1:20. The increase in the loaded Ni ratio led to an increase in active sites; however, excessive Ni aggregated and blocked the active sites of Fe_3O_4 [42]. Without the incorporation of Ni, the CO concentration was the highest, due to the reactions of hydrocarbon volatiles with the oxygen carrier (R2). Additionally, fewer H atoms were released, resulting in the highest concentrations of CH_4 and C_2H_4. As shown in Fig. 4 **(c)**, the gas HHV ranged from 15.1 to 21.0 MJ/Nm^3. The lowest gas HHV was obtained with $NiFe_5O_x$, due to the high concentration of CO_2. The highest HHV was obtained with the incorporation of $NiFe_{40}O_x$, due to the highest concentrations of C_3H_6, which had high heating values [46]. The heating value of gas obtained in this study was higher than that reported in most studies on the gasification of plastics (9.5–15.46 MJ/Nm^3), even after removing inert carrier gases in gas like N_2 or Ar [7,47].

Fig. 4 **(d)** shows the carbon and hydrogen conversion efficiencies at the vacuum stage, air introduction stage, and throughout the entire experiments. The carbon and hydrogen conversion efficiencies for the entire experiments varied within the ranges of 55.4–70.8% and 42.9–84.3%, respectively. During the vacuum stage, the carbon and hydrogen conversion efficiencies varied within the ranges of 45.3–60.1% and 37.4–78.3%, respectively. It was suggested that PP mainly decomposed during the vacuum stage, and the vacuum conditions in this stage led to a high oil yield [13]. During the vacuum stage, as the temperature increased to approximately 350–450 °C [48], large molecules broke down into H_2 and smaller hydrocarbons (R1) [49]. Then some smaller hydrocarbons reacted with the lattice oxygen in $Ni_aFe_bO_x$, generating CO, CO_2, and H_2 (R2), and some heavy hydrocarbons were purged out of the reactor and condensed into liquid oil, leading to lower carbon conversion efficiency compared to chemical looping gasification of PP with steam introduction (70.8% vs 80.2%) [7]. The Fe-Ni alloy (as shown by $NiFe_2O_4$ in Fig. 3 **(b)**) could catalyze deep cracking of hydrocarbons, leading to the formation of deposited carbon and H_2 [50]. In the air introduction stage, the deposited carbon reacted with the inlet oxygen, generating CO (R4) and CO_2 (R5), and Ni and Fe reacted with oxygen to produce NiO (R6), FeO (R7) and Fe_2O_3 (R8).

$$\text{Plastic} \rightarrow H_2 + C_yH_z \quad \text{(R1)}$$

$$C_yH_z + Ni_aFe_bO_x \rightarrow (2y - x)CO + (x - y)CO_2 + \frac{z}{2}H_2 + a\text{Ni} + b\text{Fe} \quad \text{(R2)}$$

$$C_yH_z \rightarrow yC + \frac{z}{2}H_2 \quad \text{(R3)}$$

$$C + \frac{1}{2}O_2 \rightarrow CO \quad \text{(R4)}$$

$$C + O_2 \rightarrow CO_2 \quad \text{(R5)}$$

$$\text{Ni} + \frac{1}{2}O_2 \rightarrow \text{NiO} \quad \text{(R6)}$$

$$\text{Fe} + \frac{1}{2}O_2 \rightarrow \text{FeO} \quad \text{(R7)}$$

$$\text{Fe} + \frac{3}{4}O_2 \rightarrow \frac{1}{2}Fe_2O_3 \quad \text{(R8)}$$

3.3. Effect of microwave power

Microwave power influenced the chemical looping gasification process by altering the heating rate and microwave density [15], thereby affecting gas production. Therefore, it was necessary to detail the effect of microwave power on gas production. Experiments were conducted under microwave powers of 590 W, 690 W, 790 W, 890 W, and 990 W separately to optimize the microwave power. $NiFe_{20}O_x$ was used as the oxygen carrier due to its best gas yield and H_2 yield based on Section 3.2. The obtained results are shown in Fig. 5.

3.3.1. Microwave heating performances

Fig. 5 **(a)** shows the microwave heating performances of the feedstocks using $NiFe_{20}O_x$ as oxygen carrier under different microwave powers (590 W, 690 W, 790 W, 890 W, and 990 W). The temperature of the feedstocks increased from room temperature to 900 °C in 1.5–8 min, with heating rates ranging from 112.5 to 600 °C/min. The microwave power of 990 W achieved the highest heating rate, while 590 W achieved the lowest. It should be noted that higher microwave power did not necessarily mean higher electricity consumption. Table 2 shows the energy consumption of the microwave oven at different microwave powers, ranging from 0.182 to 0.293 kWh. The highest energy consumption was recorded at 590 W, while the lowest was observed at 890 W. The reason could be attributed to the fact that lower microwave power required a longer time to heat the feedstocks to 900 °C, resulting in higher energy consumption.

3.3.2. Products distribution

Fig. 5 **(b)** shows the H_2 yield, CO yield, and gas yield obtained from the chemical looping gasification of PP using $NiFe_{20}O_x$ as the oxygen carrier under different microwave powers. The oil yield is shown in Table 1. The gas yield and oil yield varied within the ranges of 41.9–81.3 mmol/g_{PP} and 23.3–42.9 wt.%, respectively. The H_2 yield and CO yield varied within the ranges of 6.2–46.0 mmol/g_{PP} and 25.4–29.6 mmol/g_{PP}, respectively. When the microwave power increased from 590 W to 890 W, the gas yield increased. However, when the microwave power was further increased to 990 W, the gas yield decreased while the oil yield reached its highest level. Microwave power primarily affected gas yield by influencing the heating rate. As shown in Fig. 5 **(a)**, higher microwave power led to an increased heating rate, which was closely linked to heat and mass transfer within the plastics, as well as the residence time of the volatiles [32]. As the heating rate increased, the PP underwent rapid cracking, generating a significant amount of small volatile compounds. More of these volatiles escaped the reactor before undergoing secondary reactions, such as the recombination of small

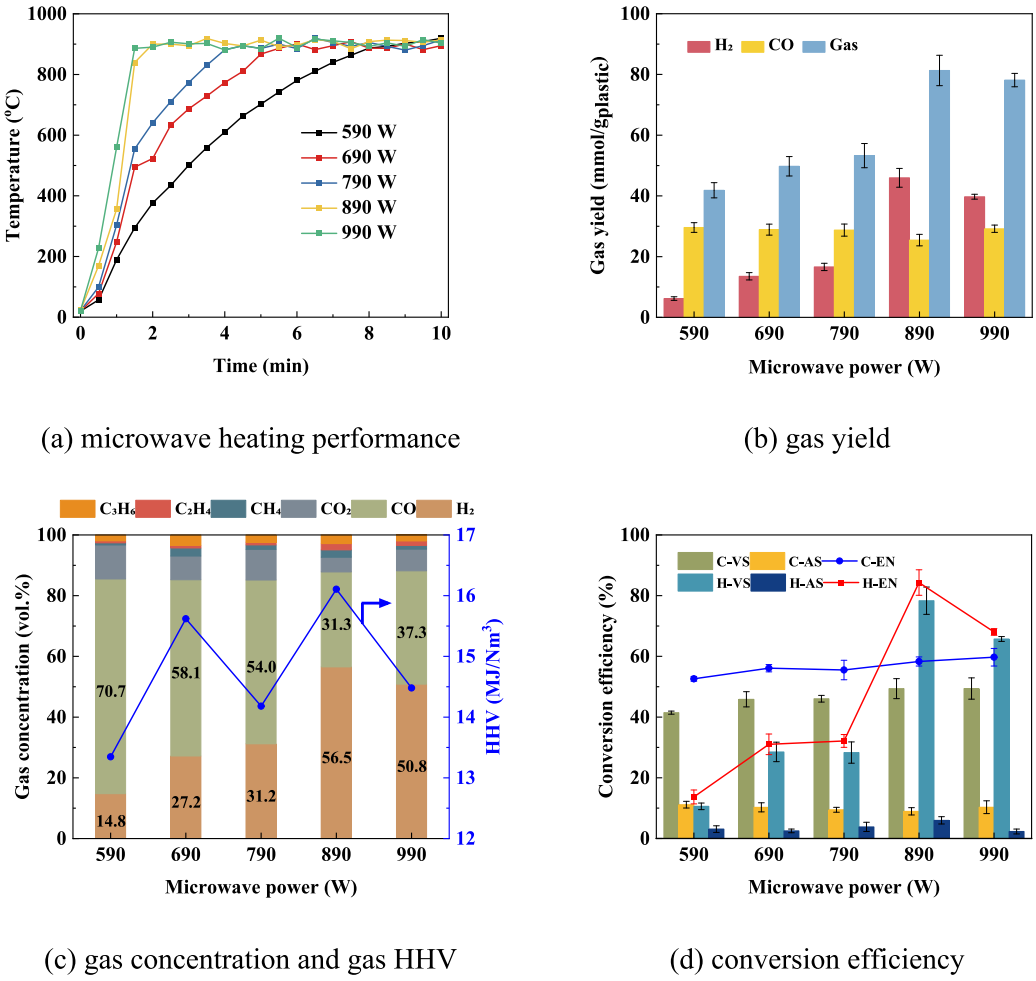

Fig. 5. Experimental results obtained from microwave-assisted chemical looping gasification of PP with different microwave powers.

Table 2
Energy consumption of microwave oven under different microwave powers.

Microwave power (W)	990	890	790	690	590
Energy consumption (kWh)	0.208	0.182	0.235	0.283	0.293

molecules [51], contributing to an increase in gas yield [16]. However, when the heating rate became excessively high, the volatiles were released too quickly, leaving insufficient time for complete cracking. Consequently, some volatiles escaped before being converted into gas products, leading to a reduction in gas yield [52]. The H_2 yield initially increased and then decreased with the increase in microwave power, while the CO yield changed slightly. At 590 W, the H_2 yield was only 6.2 mmol/g_{PP}. This was attributed to the lower heating rate, which resulted in a longer residence time and promoted the recombination reactions of small molecules [51]. As the microwave power increased, the higher heating rate reduced the recombination reactions of small molecules, thereby promoting H_2 production. The decrease in H_2 yield at 990 W was attributed to the insufficient residence time of volatiles in the reactor, caused by the excessively high heating rate, which led to the incomplete cracking of the plastic volatiles [16].

3.3.3. Gas compositions

Fig. 5 **(c)** shows the gas components and gas HHV obtained from the chemical looping gasification of PP using $NiFe_{20}O_x$ as the oxygen carrier under different microwave powers. The volume concentrations of H_2, CO, CO_2, CH_4, C_2H_4, and C_3H_6 varied within the ranges of 14.8–56.5%, 31.3–70.7%, 4.8–11.2%, 0.7–2.7%, 0.7–2.1%, and 1.9–3.4%, respectively. With the increase in microwave power, the H_2 concentration first increased then decreased, while the CO concentration showed the conversed tendency. the reason for this phenomenon had been explained in **Section 3.3.2**. The highest H_2 concentration and the lowest CO concentration was achieved at microwave power of 890 W. At 590 W, some of the heavy hydrocarbons flowed out at low temperatures and were challenging to react with lattice oxygen [33]. When the temperature was sufficiently high, the residues reacted with a surplus amount of the oxygen carrier, leading to the generation of large amounts of CO and CO_2. As the microwave power increased, more smaller hydrocarbons generated in the reactors at high temperatures reacted with the oxygen carrier (R2) [47], producing a similar amount of CO but less CO_2 due to insufficient oxygen. The highest gas yield was observed at 890 W, resulting in the lowest CO concentration. As shown in Fig. 5 **(c)**, the gas HHV ranged from 13.3 to 16.1 MJ/Nm^3. The lowest gas HHV was obtained at 590 W due to the highest concentration of CO_2. The highest HHV was obtained at 890 W due to the lowest concentration of CO_2.

Fig. 5 **(d)** shows the carbon and hydrogen conversion efficiencies at the vacuum stage, air introduction stage, and throughout the entire experiment. The carbon and hydrogen conversion efficiencies for the entire experiment varied within the ranges of 52.6–59.7% and 13.7–84.3%, respectively. During the vacuum stage, the carbon and hydrogen conversion efficiencies varied within the ranges of 41.5–49.4% and 10.6–65.7%, respectively. The carbon conversion efficiency decreased with the decrease in microwave power, due to the lower heating rate causing the breakdown of PP at lower temperatures, releasing more heavy hydrocarbons which then condensed to liquid oil

(R1) [53]. The hydrogen conversion efficiency was closely related to H_2 production due to the lower production of CH_4, C_2H_4, and C_3H_6, which could react with the oxygen carrier (R2), and the highest hydrogen conversion was achieved at 890 W.

3.4. Effect of plastic types

$NiFe_{20}O_x$ was recognized as the optimal oxygen carrier, and 890 W was found to be the most effective microwave power for maximizing gas yield. These parameters were utilized to investigate the chemical looping gasification performance of various plastics. Four prevalent plastics, representing 50.4 wt.% of global plastic production, including PP, HDPE, LDPE, and PS, were selected to examine their microwave-assisted chemical looping gasification performances [1]. LDPE and HDPE were derived from ethylene; however, LDPE had an irregular structure with numerous side chains, while HDPE had an almost linear structure with few side chains [54]. PP, synthesized from propylene, had a relatively linear structure with a methyl group ($-CH_3$) on each monomer. PS featured a linear structure with a phenyl group ($-C_6H_5$) on each monomer [55]. Additionally, mixed plastics (MP) were formulated using the global production ratios (PP: LDPE: HDPE: PS = 3.63: 2.71: 2.35: 1) to simulate real plastic waste for gas production [1]. Fig. 6 presents the results of microwave-assisted chemical looping gasification over $NiFe_{20}O_x$ under microwave power of 890 W using different plastics.

3.4.1. Products distribution

Fig. 6 **(a)** illustrates the microwave heating performance of SiC and $NiFe_{20}O_x$ mixed with various plastics under a microwave power of 890 W. The heating rates of the feedstocks were primarily determined by SiC and $NiFe_{20}O_x$, showing minimal variation based on the type of plastic, with the heating rates remaining around 450 °C/min in 2 min.

Fig. 6 **(b)** presents the H_2 yield, CO yield, and gas yield obtained from the chemical looping gasification of different plastics using $NiFe_{20}O_x$ as the oxygen carrier under a microwave power of 890 W. The oil yield is detailed in Table 1. The gas yield and oil yield varied within the ranges of 28.8–81.3 mmol/$g_{Plastic}$ and 23.3–70.0 wt.%, respectively. H_2 yield and CO yield varied within the ranges of 8.8–46.0 mmol/$g_{Plastic}$ and 15.2–38.3 mmol/$g_{Plastic}$, respectively. PS obtained the lowest gas yield, H_2 yield and CO yield, while obtained the highest oil yield. This was attributed to that PS had about 74 wt.% phenyl group (C_6H_5-) which was hard to decompose (R1) resulting in the higher oil yield. Previous studies reported a gas yield of only 24.4 wt.% from PS pyrolysis at 900 °C [56]. LDPE and HDPE showed similar H_2 yields, while HDPE exhibited a higher CO yield. This was attributed to HDPE's linear structure, which consisted of shorter and more regular molecular chains, requiring higher temperatures or longer reaction times for complete cracking [57]. Under these conditions, the carbonaceous fragments produced are more likely to oxidize into CO at the elevated temperature of 900 °C. In contrast, PP, with its lower crystallinity and more regular side chains, is more susceptible to thermal decomposition, resulting in its higher gas and H_2 yields [58]. The synergistic effect of MP was not conducive to gas

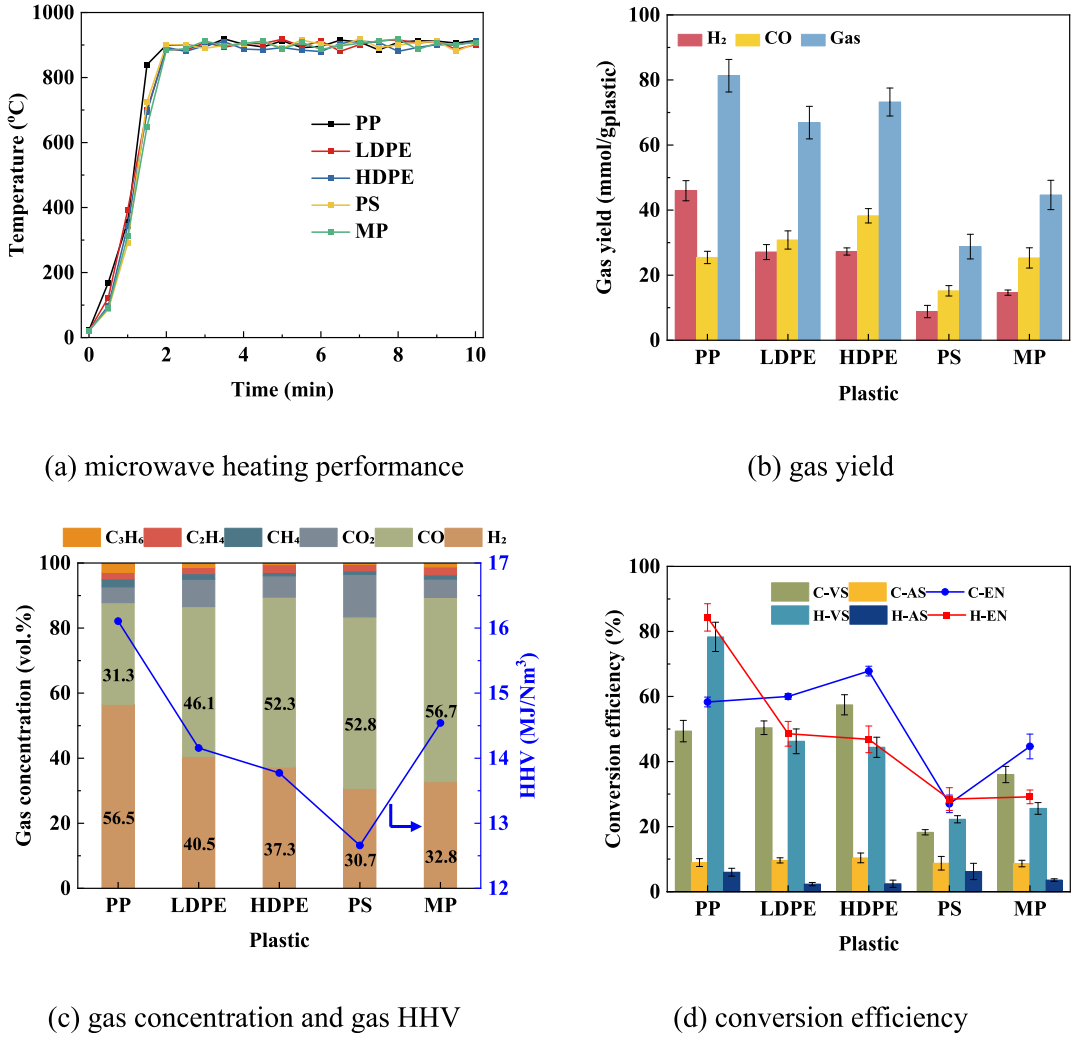

Fig. 6. Experimental results obtained from microwave-assisted chemical looping gasification of different plastics.

production. This was evident as the gas yield (44.7 mmol/$g_{Plastic}$) significantly decreased compared to the average value (70.0 mmol/$g_{Plastic}$) of the different plastics, while the oil yield (44.7 wt.%) significantly increased compared to the weighted average value (30.1 wt.%). This was attributed to secondary reactions occurring in the generated vapors between the different plastics [53], resulting in a higher oil yield. These average values were calculated based on the weight percentages of different plastics in the MP.

3.4.2. Gas compositions

Fig. 6 **(c)** shows the gas components and gas HHV obtained from the chemical looping gasification of different plastics using $NiFe_{20}O_x$ as the oxygen carrier under a microwave power of 890 W. The volume concentrations of H_2, CO, CO_2, CH_4, C_2H_4, and C_3H_6 varied within the ranges of 30.7–56.5%, 31.3–56.7%, 4.8–13.1%, 1.1–2.4%, 2.0–2.4%, and 0.4–2.8%, respectively. PS showed the highest CO concentration and the lowest H_2 concentration among different plastics, attributed to the difficulty in breaking benzene rings [56]. The carbon and hydrogen atoms in the gas mainly originated from the ethylene side chains of styrene, which contained fewer hydrogen atoms, resulting in the lowest H_2 concentration. HDPE and LDPE had similar H_2 concentrations, while HDPE showed a higher CO concentration. MP exhibited the highest CO concentration, which was due to the largest amounts of heavy molecules flowing out and the residues reacting with the surplus oxygen carrier (R2), leading to the highest CO concentration. As shown in Fig. 6 **(c)**, the gas HHV ranged from 12.7 to 16.1 MJ/Nm^3. The lowest gas HHV was observed with PS, due to its highest CO_2 concentration (13.1 vol.%), while PP showed the highest gas HHV with the lowest CO_2 concentration (4.9 vol.%).

Fig. 6 **(d)** shows the carbon and hydrogen conversion efficiencies during the vacuum stage, air introduction stage, and throughout the entire experiment. The carbon and hydrogen conversion efficiencies for the entire experiment varied within the ranges of 27.0–67.8% and 28.5–84.3%, respectively. During the vacuum stage, the carbon and hydrogen conversion efficiencies varied within the ranges of 18.3–57.4% and 22.3–78.3%, respectively. PS achieved the lowest carbon and hydrogen conversion efficiencies, due to its highest oil yield (70 wt.%). HDPE showed higher carbon conversion efficiency and similar hydrogen conversion efficiency compared to LDPE, due to its more regular molecular chains, which required higher temperatures or longer reaction times for complete cracking [57], making it more likely to produce CO.

3.5. Result comparisons

Table 3 presents the experimental results for gas production from the pyrolysis and gasification of PP, along with the findings of this study. The optimal gas yield in this study was 81.3 mmol/g_{PP} (1.15 g/g_{PP}), achieved using $NiFe_{20}O_x$ as the oxygen carrier at a microwave power of 890 W and a reaction temperature of 900 °C. In comparison to electrical air gasification of PP, the gas yield in this study was lower (1.15 g/g_{PP} vs. 1.66 g/g_{PP}) [59], which can be attributed to the slower release rate of lattice oxygen [60]. However, the H_2 concentration in this study was significantly higher (56.5 vol.% vs. 11.2 vol.%) due to the catalytic effect of $NiFe_{20}O_x$. In air gasification, the introduction of air diluted the generated gas, leading to a lower heating value of 7.92 MJ/Nm^3 compared to 16.1 MJ/Nm^3 in this study [59]. Similarly, microwave-assisted gasification of PP produced a lower H_2 concentration and heating value [61]. The H_2 concentration observed in this study (56.5 vol.%) was slightly lower than that reported for PP pyrolysis (59.0 vol.%), likely due to the use of a more complex catalyst in the pyrolysis process and the oxidation of lattice oxygen in this study [34]. Nevertheless, the gas yield in this study was significantly higher, owing to the oxidation of plastic volatiles, which enhanced H_2 production. In microwave pyrolysis of PP without a catalyst, both the gas yield and H_2 concentration were lower than in this study [62].

4. Conclusions

In this study, microwave-assisted heating coupled with chemical looping gasification of plastics at 900 °C were investigated, detailing the effects of Ni/Fe molar ratio of $Ni_aFe_bO_x$ oxygen carrier, microwave power, and types of plastics on gas production. Investigations first screened Ni/Fe molar ratios (0, 1:40, 1:20, 1:10, 3:20, and 1:5) in the $Ni_aFe_bO_x$ oxygen carrier. $NiFe_{20}O_x$ emerged as the optimal oxygen carrier, achieving the highest gas yield of 81.3 mmol/g_{PP} and an H_2 yield of 46.0 mmol/g_{PP}, with a hydrogen conversion efficiency of up to 84.3 %. Using Fe_3O_4 as the oxygen carrier, the highest gas HHV of 21 MJ/Nm^3 and the highest carbon conversion efficiency of 70.9 % were obtained.

Subsequently, the effect of microwave powers (590 W, 690 W, 790 W, 890 W, and 990 W) on gas production was examined. The gas yield first increased then decreased with increasing microwave power, identifying 890 W as the optimal power. The average heating rate ranged from 112.5 to 600 °C/min across the different microwave powers, with the electrical power consumption of the microwave oven varying between 0.182 kWh and 0.293 kWh. Notably, the microwave power of 890 W resulted in the lowest electrical power consumption.

Using the optimal microwave power of 890 W, the chemical looping gasification performances of different plastics over $NiFe_{20}O_x$ were investigated. PP showed the highest gas yield and H_2 yield, while HDPE exhibited the highest carbon conversion efficiency of 67.8 % and the highest CO yield of 38.3 mmol/$g_{Plastic}$. However, the synergistic effect of MP was not conducive to gas production. This was attributed to secondary reactions occurring in the generated vapors between different plastics, resulting in a high oil yield.

CRediT authorship contribution statement

Wenming Fu: Writing – original draft. **Yaning Zhang:** Supervision, Funding acquisition. **Weitao Cao:** Validation. **Wenke Zhao:** Validation. **Bingxi Li:** Supervision.

Declaration of competing interest

The authors declare that they have no known competing financial interests or personal relationships that could have appeared to influence the work reported in this paper.

Table 3
Gas production from thermochemical conversion of PP.

Methods	Main conditions	Gas yield (g/g_{PP})	Compositions (vol.%)					Ref
			H_2	CH_4	CO	CO_2	others	
Microwave-assisted chemical looping	890 W, 900 °C, $NiFe_{20}O_x$	1.15	56.5	2.4	31.3	4.8	7.4	This study
Electrical air gasification	703 °C	1.66	11.2	11.4	43.3	26.1	8.0	[59]
Microwave-assisted air gasification	800 W, 900 °C, SiC	0.86	7.2	5.4	25.7	9.8	51.9	[61]
Electrical pyrolysis	900 °C, NiCo/ZSM-5	0.65	59.0	13.5	/	/	27.5	[34]
Microwave-assisted pyrolysis	1000 W, 900 °C, SiC	0.71	11.2	12.0	/	/	76.8	[62]

Data availability

Data will be made available on request.

Acknowledgements

This work was financially supported by the National Natural Science Foundation of China (52076049), Heilongjiang Province "Double First-class" Discipline Collaborative Innovation Achievement Project (LJGXCG2023-080), and Heilongjiang Provincial Key R&D Program (2023ZX02C05).

References

[1] Plastics Europe, Plastics - the fast facts 2023, https://plasticseurope.org/knowledge-hub/plastics-the-fast-facts-2023/, 2023.
[2] T. Pan, H. Liao, F. Yang, F. Sun, Y. Guo, H. Yang, D. Feng, X. Zhou, Q. Wang, Review of microplastics in lakes: sources, distribution characteristics, and environmental effects, Carbon Res. 2 (2023) 25.
[3] Y. Chen, Y. Li, X. Liang, S. Lu, J. Ren, Y. Zhang, Z. Han, B. Gao, K. Sun, Effects of microplastics on soil carbon pool and terrestrial plant performance, Carbon Res. 3 (2024) 1–23.
[4] G. Lopez, M. Artetxe, M. Amutio, J. Alvarez, J. Bilbao, M. Olazar, Recent advances in the gasification of waste plastics. A Critical Overview, Renew. Sustain. Energy Rev. 82 (2018) 576–596.
[5] A.A. Arpia, T.B. Nguyen, W.H. Chen, C.D. Dong, Y.S. Ok, Microwave-assisted gasification of biomass for sustainable and energy-efficient biohydrogen and biosyngas production: a state-of-the-art review, Chemosphere 287 (2022) 132014.
[6] Z. Li, J. Li, T. Yu, X. Jia, J. Zhao, B. Yan, G. Chen, Chemical looping gasification of high-moisture content biomass: the interactions between H_2O and oxygen carrier, Appl. Energy 368 (2024) 123529.
[7] S. Wu, Z. Ren, Q. Hu, D. Yao, H. Yang, Upcycling plastic waste into syngas by staged chemical looping gasification with modified Fe-based oxygen carriers, Appl. Energy 353 (2024) 122105.
[8] S. Wang, F. Wu, X. Wang, Experimental and kinetics analysis on biomass chemical looping gasification using lean iron ore as oxygen carrier, Chem. Eng. J. 474 (2023) 145855.
[9] Y. Liu, K. Yin, J. Wu, D. Mei, J. Konttinen, T. Joronen, Z. Hu, C. He, Ash chemistry in chemical looping process for biomass valorization: a review, Chem. Eng. J. 478 (2023) 147429.
[10] A. Goel, E.M. Moghaddam, W. Liu, C. He, J. Konttinen, Biomass chemical looping gasification for high-quality syngas: a critical review and technological outlooks, Energ. Conver. Manage. 268 (2022) 116020.
[11] W. Fu, Y. Zhang, L. Cui, H. Liu, T. Maqsood, Experimental microwave-assisted air gasification of biomass in fluidized bed reactor, Bioresour. Technol. 369 (2023) 128378.
[12] A.A. Arpia, W.H. Chen, S.S. Lam, P. Rousset, M.D.G. de Luna, Sustainable biofuel and bioenergy production from biomass waste residues using microwave-assisted heating: a comprehensive review, Chem. Eng. J. 403 (2021) 126233.
[13] S. Fan, Y. Zhang, L. Cui, Q. Xiong, T. Maqsood, Conversion of polystyrene plastic into aviation fuel through microwave-assisted pyrolysis as affected by iron-based microwave absorbents, ACS Sustain. Chem. Eng. 11 (2023) 1054–1066.
[14] X. Fan, B. Li, W. Zi, M. Kang, H. Wu, J. Bian, M. Sun, Microwave dielectric characterization and loss mechanism of biowaste during pyrolysis, Energ. Conver. Manage. 301 (2024) 118075.
[15] W. Fu, J. Dai, Y. Zhang, M. Guang, Y. Liu, B. Li, Heating performances of high density polyethylene (HDPE) plastic particles in a microwave chamber, Sustainable Energy Technol. Assess. 48 (2021) 101581.
[16] R.K. Singh, B. Ruj, A.K. Sadhukhan, P. Gupta, Impact of fast and slow pyrolysis on the degradation of mixed plastic waste: product yield analysis and their characterization, J. Energy Inst. 92 (2019) 1647–1657.
[17] H. Li, J. Xu, S. Mbugua Nyambura, J. Wang, C. Li, X. Zhu, X. Feng, Y. Wang, Food waste pyrolysis by traditional heating and microwave heating: a review, Fuel 324 (2022) 124574.
[18] F. An, D. Chen, Z. Zhong, X. Wang, Experimental investigation of the effect of microwave power on the chemical looping gasification of aquatic plant water hyacinth, J. Energy Inst. 114 (2024) 101537.
[19] S. Daneshmand-Jahromi, M.H. Sedghkerdar, N. Mahinpey, A review of chemical looping combustion technology: fundamentals, and development of natural, industrial waste, and synthetic oxygen carriers, Fuel 341 (2023) 127626.
[20] X. Zhang, F. Zhang, Z. Song, L. Lin, X. Zhao, J. Sun, Y. Mao, W. Wang, Review of chemical looping process for carbonaceous feedstock conversion: rational design of oxygen carriers, Fuel 325 (2022) 124964.
[21] C. Lu, K. Li, H. Wang, X. Zhu, Y. Wei, M. Zheng, C. Zeng, Chemical looping reforming of methane using magnetite as oxygen carrier: Structure evolution and reduction kinetics, Appl. Energy 211 (2018) 1–14.
[22] Z. Ma, R. Xiao, L. Chen, Redox reaction induced morphology and microstructure evolution of iron oxide in chemical looping process, Energ. Conver. Manage. 168 (2018) 288–295.
[23] L. Hou, Q. Yu, K. Wang, Z. Qi, Q. Qin, T. Wu, Optimal synthesis of $YBaCo_4O_7$ oxygen carrier for chemical looping air separation, Energy Sour. Part A 40 (2018) 2354–2366.
[24] Z. Yu, Y. Yang, S. Yang, Q. Zhang, J. Zhao, Y. Fang, X. Hao, G. Guan, Iron-based oxygen carriers in chemical looping conversions: a review, Carbon Resour. Convers. 2 (2019) 23–34.
[25] D. Xu, B. Wang, X. Li, Y.W. Cheng, W. Fu, Y. Dai, C.H. Wang, Solar-driven biomass chemical looping gasification using Fe_3O_4 for syngas and high-purity hydrogen production, Chem. Eng. J. 479 (2024) 147901.
[26] Z. Peng, Z. Li, X. Lin, M. Yang, J.Y. Hwang, Y. Zhang, G. Li, T. Jiang, Microwave power absorption in materials for ferrous metallurgy, JOM 69 (2016) 178–183.
[27] S. Ma, M. Li, G. Wang, L. Zhang, S. Chen, Z. Sun, J. Hu, M. Zhu, W. Xiang, Effects of Zr doping on Fe_2O_3/CeO_2 oxygen carrier in chemical looping hydrogen generation, Chem. Eng. J. 346 (2018) 712–725.
[28] C.H. Wu, C. Liu, D. Su, H.L. Xin, H.T. Fang, B. Eren, S. Zhang, C.B. Murray, M. B. Salmeron, Bimetallic synergy in cobalt–palladium nanocatalysts for CO oxidation, Nat. Catal. 2 (2018) 78–85.
[29] Y. Qiu, S. Zhang, D. Cui, M. Li, J. Zeng, D. Zeng, R. Xiao, Enhanced hydrogen production performance at intermediate temperatures through the synergistic effects of binary oxygen carriers, Appl. Energy 252 (2019) 113454.
[30] Z. Huang, Z. Deng, F. He, D. Chen, G. Wei, K. Zhao, A. Zheng, Z. Zhao, H. Li, Reactivity investigation on chemical looping gasification of biomass char using nickel ferrite oxygen carrier, Int. J. Hydrogen Energy 42 (2017) 14458–14470.
[31] Y. Khani, S. Valizadeh, H. Yim, W.H. Chen, C. Hyun Ko, S. Hoon Lee, S.C. Jung, Y. K. Park, Upgrading of plastic waste-derived wax through air gasification using promoted Ni/Al_2O_3 catalysts for H_2 generation, Chem. Eng. J. 477 (2023) 147053.
[32] M. Zhang, Y. Qi, W. Zhang, M. Wang, J. Li, Y. Lu, S. Zhang, J. He, H. Cao, X. Tao, H. Xu, S. Zhang, A review on waste tires pyrolysis for energy and material recovery from the optimization perspective, Renew. Sustain. Energy Rev. 199 (2024) 114531.
[33] Z. Cui, Y. Sun, J. Zhang, B. Liu, W. Tian, Multi-level optimization of biomass chemical looping gasification process based on composite oxygen carrier, Chem. Eng. Sci. 287 (2024) 119727.
[34] W. Fu, Y.W. Cheng, D. Xu, Y. Zhang, C.H. Wang, Reaction synergy of bimetallic catalysts on ZSM-5 support in tailoring plastic pyrolysis for hydrogen and value-added product production, Appl. Energy 372 (2024) 123853.
[35] J. Luo, G. Gong, R. Ma, S. Sun, C. Cui, H. Cui, J. Sun, N. Ma, Study on high-value products of waste plastics from microwave catalytic pyrolysis: construction and performance evaluation of advanced microwave absorption-catalytic bifunctional catalysts, Fuel 346 (2023) 128296.
[36] J. Liu, J. Wei, X. Feng, M. Song, S. Shi, S. Liu, G. Liu, Ni/HZSM-5 catalysts for hydrodeoxygenation of polycarbonate plastic wastes into cycloalkanes for sustainable aviation fuels, Appl. Catal. B 338 (2023) 123050.
[37] F. Hossain, J.V. Turner, R. Wilson, L. Chen, G. de Looze, S.W. Kingman, C. Dodds, G. Dimitrakis, State-of-the-art in microwave processing of metals, metal powders and alloys, Renew. Sustain. Energy Rev. 202 (2024) 114650.
[38] X. Jie, W. Li, D. Slocombe, Y. Gao, I. Banerjee, S. Gonzalez-Cortes, B. Yao, H. AlMegren, S. Alshihri, J. Dilworth, J. Thomas, T. Xiao, P. Edwards, Microwave-initiated catalytic deconstruction of plastic waste into hydrogen and high-value carbons, Nat. Catal. 3 (2020) 902–912.
[39] J. Hu, S. Chen, W. Xiang, Ni, Co and Cu-promoted iron-based oxygen carriers in methane-fueled chemical looping hydrogen generation process, Fuel Process. Technol. 221 (2021) 106917.
[40] Z. Chen, W. Wei, X. Chen, Y. Liu, Y. Shen, B.J. Ni, Upcycling of plastic wastes for hydrogen production: advances and perspectives, Renew. Sustain. Energy Rev. 195 (2024) 114333.
[41] Y. Wang, Y. Wen, W. Su, W. Fu, C.H. Wang, Carbon deposition behavior on biochar during chemical vapor deposition process, Chem. Eng. J. 485 (2024) 149726.
[42] C.C. Chong, S.N. Bukhari, Y.W. Cheng, H.D. Setiabudi, A.A. Jalil, C. Phalakornkule, Robust Ni/Dendritic fibrous SBA-15 (Ni/DFSBA-15) for methane dry reforming: effect of Ni loadings, Appl. Catal. A 584 (2019) 117174.
[43] Y. Cui, Y. Zhang, L. Cui, Q. Xiong, E. Mostafa, Microwave-assisted fluidized bed reactor pyrolysis of polypropylene plastic for pyrolysis gas production towards a sustainable development, Appl. Energy 342 (2023) 121099.
[44] Y. Li, M.A. Nahil, P.T. Williams, Pyrolysis-catalytic steam reforming of waste plastics for enhanced hydrogen/syngas yield using sacrificial tire pyrolysis char catalyst, Chem. Eng. J. 467 (2023) 143427.
[45] J. Du, M. Wu, S. Chen, W. Xiang, Interactions of Mg-Fe-Al-O oxygen carriers with rare earth dopants (Ce, Y, Sm, La, and Pr) in chemical looping steam reforming, Fuel 361 (2024) 130606.
[46] L. Fan, Z. Su, J. Wu, Z. Xiao, P. Huang, L. Liu, H. Jiang, W. Zhou, S. Liu, R. Ruan, Integrating continuous-stirred microwave pyrolysis with ex-situ catalytic upgrading for linear low-density polyethylene conversion: Effects of parameter conditions, J. Anal. Appl. Pyrol. 157 (2021) 105213.
[47] P.C. Chiu, Y. Ku, H.C. Wu, Y.L. Kuo, Y.H. Tseng, Chemical looping combustion of polyurethane and polypropylene in an annular dual-tube moving bed reactor with iron-based oxygen carrier, Fuel 135 (2014) 146–152.
[48] Y. Cui, Y. Zhang, L. Cui, Y. Liu, B. Li, W. Liu, Microwave-assisted pyrolysis of polypropylene plastic for liquid oil production, J. Clean. Prod. 411 (2023) 137303.
[49] W. Fu, Y.W. Cheng, Y. Wang, Y. Zhang, C.H. Wang, Counteractive catalytic effects of FeNi- versus Fe- and Ni- in plastic pyrolysis for advanced-quality jet fuel production, Chem. Eng. J. 494 (2024) 153078.
[50] D. Yao, C.H. Wang, Pyrolysis and in-line catalytic decomposition of polypropylene to carbon nanomaterials and hydrogen over Fe-and Ni-based catalysts, Appl. Energy 265 (2020) 114819.
[51] J. Luo, S. Sun, X. Chen, J. Lin, R. Ma, R. Zhang, L. Fang, In-depth exploration of the energy utilization and pyrolysis mechanism of advanced continuous microwave pyrolysis, Appl. Energy 292 (2021) 116941.

[52] R.K. Singh, B. Ruj, Time and temperature depended fuel gas generation from pyrolysis of real world municipal plastic waste, Fuel 174 (2016) 164–171.
[53] W.H. Chen, P. Pratim Biswas, E.E. Kwon, Y.K. Park, S. Rajendran, L. Gnanasekaran, J.S. Chang, Optimization of the process parameters of catalytic plastic pyrolysis for oil production using design of experiment approaches: a review, Chem. Eng. J. 471 (2023) 114695.
[54] I. Oluwoye, L.L. Machuca, S. Higgins, S. Suh, T.S. Galloway, P. Halley, S. Tanaka, M. Iannuzzi, Degradation and lifetime prediction of plastics in subsea and offshore infrastructures, Sci. Total Environ. 904 (2023) 116719.
[55] H. Bin, S. Wang, J. Yan, H. Zhang, L. Qiu, W. Liu, Y. Guo, J. Shen, C. Bin, C. Shi, X. Ge, Review of waste plastics treatment and utilization: efficient conversion and high value utilization, Process Saf. Environ. Prot. 183 (2024) 378–398.
[56] I.I. Ahmed, A.K. Gupta, Hydrogen production from polystyrene pyrolysis and gasification: characteristics and kinetics, Int. J. Hydrogen Energy 34 (2009) 6253–6264.
[57] S.D. Anuar Sharuddin, F. Abnisa, W.M.A. Wan Daud, M.K. Aroua, A review on pyrolysis of plastic wastes, Energ. Conver. Manage. 115 (2016) 308–326.
[58] Y. Peng, Y. Wang, L. Ke, L. Dai, Q. Wu, K. Cobb, Y. Zeng, R. Zou, Y. Liu, R. Ruan, A review on catalytic pyrolysis of plastic wastes to high-value products, Energ. Conver. Manage. 254 (2022) 115243.
[59] R. Xiao, B. Jin, H. Zhou, Z. Zhong, M. Zhang, Air gasification of polypropylene plastic waste in fluidized bed gasifier, Energ. Conver. Manage. 48 (2007) 778–786.
[60] J. Zhao, Y. Song, D. Li, Z. Xie, Y. Ren, L. Kong, X. Fan, X. Xiao, J. Li, Z. Zhao, Strong NiO_x and ZrO_2 interactions to eliminate the inhibiting effect of trace oxygen for propane dehydrogenation by accelerating lattice oxygen releasing, Appl. Catal. A 661 (2023) 119246.
[61] Y. Cui, H. Shi, Y. Zhang, L. Cui, W. Zhao, W. Liu, Experimental investigation on air gasification of polypropylene particles in a microwave fluidized bed reactor, Ind. Eng. Chem. Res. 62 (2023) 17306–17313.
[62] H. Shi, Y. Cui, Y. Zhang, W. Zhao, W. Liu, R. Ruan, Gases production from microwave-assisted pyrolysis of polypropylene plastic, J. Environ. Chem. Eng. 11 (2023) 110851.